Unusual Intensities in the Resonance Raman Spectra and Excitation Profiles of an Intervalence Metal-to-Metal Charge Transfer Complex

Jeffrey L. Wootton and Jeffrey I. Zink*

Contribution from the Department of Chemistry and Biochemistry, University of California, Los Angeles, Los Angeles, California 90095

Received July 1, 1996. Revised Manuscript Received November 2, 1996[⊗]

Abstract: The resonance Raman spectra of the metal-to-metal charge transfer (MMCT) mixed-valence complex $[(OC)_5Cr^0-CN-Os^{III}(NH_3)_5](CF_3SO_3)_2$ are measured and analyzed. The excitation profiles (the Raman intensities as a function of excitation wavelength) are obtained using the SO_3 stretch of the triflate ion as an internal standard. The ratios of the Raman intensities are not constant with different excitation wavelengths. This unusual observation is attributed to interference between two overlapping electronic states of the molecule. The electronic states are observed in the low-temperature polarized single crystal absorption spectrum. The resonance Raman intensities and excitation profiles are calculated with the time dependent theory of spectroscopy and include the interference between the electronic states. The origin of the unusual intensities is quantitatively explained in terms of the real and imaginary parts of the Raman cross sections from the two states.

Introduction

Spectroscopic studies of electron transfer continue to be a very active area of research. Recent review articles chronicled many contemporary issues in electron transfer research[1,2] including the use of resonance Raman intensities to obtain mode specific vibrational reorganization energies for electron transfer reactions.[1] The vibrational reorganization energies are related to the displacement of the excited state potential energy surface relative to the ground state surface along a configurational coordinate. The displacements or excited state distortions are calculated from the resonance Raman intensities of the normal modes of vibration. This method has been applied to many electron transfer systems including biologically important molecules,[3−7] noncovalent donor−acceptor complexes,[8,9] ligand-to-ligand charge transfer (LLCT),[10] and mixed-valence molecules with metal-to-metal intervalence charge transfer (MMCT)[11−14] electronic transitions.

In many of these studies, the ratios of the distortions were calculated from the measured intensities by using the Savin formula

$$\frac{I_k}{I_{k'}} = \left(\frac{\Delta_k \omega_k}{\Delta_{k'} \omega_{k'}}\right)^2 \qquad (1)$$

where I_k is the resonance Raman intensity, Δ_k is the distortion, and ω_k is the vibrational frequency of the k′th mode.[15−17] This equation assumes that only one excited electronic surface is involved and is most accurate in the preresonance region (short time dynamics). The individual distortions are calculated from the ratios by using the absorption band width, and the reorganization energies are calculated from the distortions by multiplying by the vibrational frequency. When eq 1 is valid, the ratios of intensities are constant when the exciting laser is in resonance throughout the absorption band.

The most common cause of failure of the validity of eq 1 is structure in the resonance Raman profiles caused by longer time wavepacket dynamics.[18−22] The consequences of these effects are illustrated in Figure 1. When short time wavepacket dynamics occur on one surface, the resonance Raman excitation profiles are structureless as shown in the top panel of Figure 1 and have an overall shape that follows that of the electronic absorption spectrum. Figure 1 illustrates the profiles for two modes that play a major role in this paper and show the behavior expected if only one electronic state is involved. The profiles are nested and the ratios of the intensities at every excitation wavelength are the same.

When longer time dynamics occur, the profiles will develop structure as shown in the bottom panel of Figure 1. The structure is similar to vibronic structure in absorption spectra and has a spacing corresponding to the vibrational frequency

[⊗] Abstract published in *Advance ACS Abstracts,* January 15, 1997.

(1) Myers, A. B. *Chem. Rev.* **1996**, *96*, 911.
(2) Barbara, P. F.; Meyer, T. J.; Ratner, M. A. *J. Phys. Chem.* **1996**, *100*, 13148.
(3) Rush, T., III; Kumble, R.; Mukherjee, A.; Blackwood, M. E. Jr.; Spiro, T. G. *J. Phys. Chem.* **1996**, *100*, 12076.
(4) Fraga, E.; Webb, M. A.; Loppnow, G. R. *J. Phys. Chem.* **1996**, *100*, 3278.
(5) Wright, P. G.; Stein, P.; Burke, J. M.; Spiro, T. G. *J. Am. Chem. Soc.* **1979**, *101*, 3531.
(6) Peticolas, W. L.; Strommen, D. P.; Lakshminarayanan, V. *J. Chem. Phys.* **1980**, *73*, 4185.
(7) Peticolas, W. L.; Rush, T., III *J. Comp. Chem.* **1995**, *16*, 1261.
(8) Markel, F.; Ferris, N. S.; Gould, I. R.; Myers, A. B. *J. Am. Chem. Soc.* **1992**, *114*, 6208.
(9) Britt, B. M.; McHale, J. L.; Friedrich, D. M. *J. Phys. Chem.* **1995**, *99*, 6347.
(10) Wootton, J. L.; Zink, J. I. *J. Phys. Chem.* **1995**, *99*, 7251.
(11) Doorn, S. K.; Hupp, J. T. *J. Am. Chem. Soc.* **1989**, *111*, 1142.
(12) (a) Doorn, S. K.; Blackbourn, R. L.; Johnson, C. S.; Hupp, J. T. *Electrochim. Acta* **1991**, *36*, 1775. (b) Petrov, V.; Hupp, J. T.; Mottley, C.; Mann, L. C. *J. Am. Chem. Soc.* **1994**, *116*, 2171.
(13) Lu, H.; Petrov, V.; Hupp, J. T. *Chem. Phys. Lett.* **1995**, *235*, 521.
(14) Pfennig, B. W.; Wu, Y.; Kumble, R.; Spiro, T. G.; Bocarsly, A. B. *J. Phys. Chem.* **1996**, *100*, 5745.
(15) Heller, E. J.; Sundberg, R. L.; Tannor, D. J. *J. Phys. Chem.* **1982**, *86*, 1822.
(16) Warshel, A.; Dauber, P. *J. Chem. Phys.* **1977**, *66*, 5477.
(17) Tang, J.; Albrecht, A. C.; *Raman Spectroscopy, Vol. 2,* H. Szynanski, H, Ed.; Plenum Press: New York, 1970; Vol. 2, p. 33.
(18) Heller, E. J. *Acc. Chem. Res.* **1981**, *14*, 368.
(19) Tannor, D. J.; Heller, E. J. *J. Phys. Chem.* **1982**, *77*, 202.
(20) Heller, E. J.; Sundberg, R. L.; Tannor, D. J. *J. Phys. Chem.* **1982**, *86*, 1822.
(21) Lee, S. Y.; Heller, E. J. *J. Chem. Phys.* **1979**, *71*, 4777.
(22) Zink, J. I.; Shin, K. S. K. *Adv. Photochem.* **1991**, *16*, 119.

S0002-7863(96)02228-7 CCC: $14.00

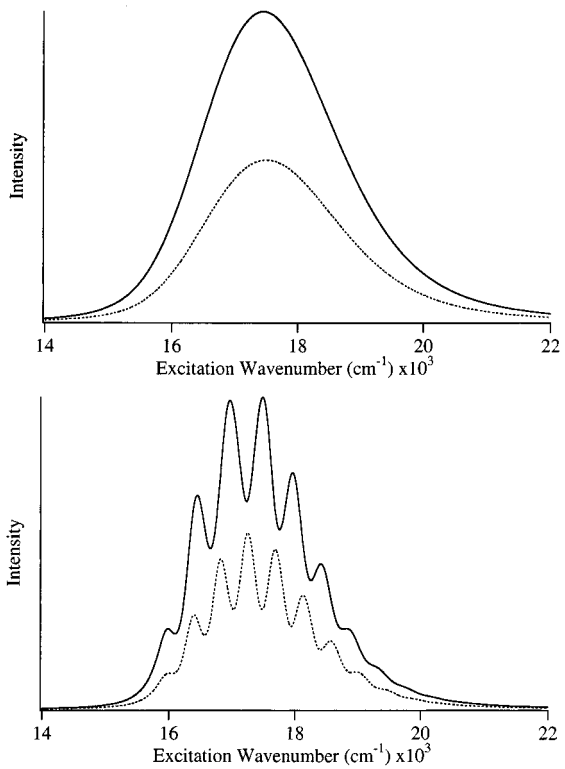

Figure 1. Resonance Raman excitation profiles calculated for short time dynamics (top, $\Gamma = 750$ cm^{-1}) and long time dynamics (bottom, $\Gamma = 200$ cm^{-1}). The two modes have frequencies of 396 (solid lines) and 488 cm^{-1} (dashed lines.) The distortions are $\Delta_{396} = 2.2$ and $\Delta_{488} = 1.3$.

of the mode in the excited electronic state. The profiles are still nested and still have an overall shape that follows that of the absorption spectrum. However, the ratio of the intensities will change as the excitation wavelength is changed. For example, if the ratio is measured at 17 100 cm^{-1} where the profile of the 488- cm^{-1} mode has a peak but that of the 396-cm-^{1} mode has a minimum, the ratio will be larger than that measured at 17 400 cm^{-1} where the first mode has a minimum and the second has a peak. The ratios oscillate around a mean value that is the constant ratio found in the top panel, but a measurement at any one wavenumber may be misleading.

A less common cause of the failure of eq 1 is interference between multiple electronic states.[23,24] Equation 1 and the spectra in Figure 1 can only be correct when there is only one excited state (and the appropriate time conditions). When two or more excited states are nearby in energy, constructive and destructive interference can occur leading to large and unexpected changes in the Raman intensities. These changes may totally change the shapes of the excitation profiles. For example, resonance de-enhancement in resonance Raman excitation profiles was treated using the time-dependent theory and considering interference between two electronic states.[23] The effects of the transition dipole moment of the two states, the displacements of the normal coordinates in the two states, the energy separation of the two states, and the damping factors were calculated and interpreted. Resonance de-enhancement in resonance Raman excitation profiles of the low-frequency vibrational modes in the trinuclear mixed-valence complex $[(NC)_5FeCN-Pt(NH_3)_4NC-Fe(CN)_5]^{4-}$ was recently reported and interpreted using time-dependent theory.[14]

In the course of measuring the resonance Raman excitation profiles of the MMCT complex $[(CO)_5Cr^0-CN-Os^{III}(NH_3)_5](CF_3SO_3)_2$, (CrOs),[25] we found dramatic variation of resonance Raman intensity ratios with different excitation wavelengths in the intervalence absorption band. The shapes of the resonance Raman excitation profiles are very different from that of the absorption band. We explain these unusual observations as interference between two electronic states of the molecule and verify the existence of these states in the low-temperature polarized single-crystal absorption spectrum. We calculate the resonance Raman excitation profiles using the time-dependent theory and interpret the results in terms of interference between the two electronic states.

Experimental Section

Resonance Raman spectra were recorded by excitation with the 457.9-, 488-, and 514.5-nm lines of an argon ion laser (Coherent Innova 90−6) and the 530.9-, 568.2-, 647.1-, and 676.4-nm lines of a krypton ion laser (Coherent Innova 90-K). The samples were diluted in KBr (1 mg of sample/250 mg of KBr) and cooled to 20 K with a closed cycle helium refrigerator (Air Products Displex) to minimize thermal degradation. The Raman-scattered light was dispersed through a triple monochromator (Instruments SA, Inc., Models DHR320 and HR640) and detected by a charge coupled device, CCD (Princeton Research). The wavelength was calibrated using the emission of a neon bulb. The intensities were measured by taking the integrated area of each Raman band. For the resonance Raman excitation profiles, the Raman intensities were measured relative to the intensity of the 1040-cm^{-1} Raman band from the triflate counterion.

Single crystals of CrOs were grown between quartz plates by the slow evaporation of an aqueous solution. The 77 K single-crystal polarized absorption spectrum was recorded on a locally constructed instrument previously described in the literature.[26]

Results

Resonance Raman Excitation Profiles. The resonance Raman excitation profiles for the 396-, 488-, 2054-, and 2100-cm^{-1} modes of CrOs are shown in Figure 2. The excitation profiles are plots of the ratio of the intensity of the specified normal mode to the intensity of the 1040-cm^{-1} mode of the triflate standard versus the excitation frequency.

Two features of the profiles are noteworthy. First, the profiles consist of two components with a pronounced intensity decrease in the middle. Their shapes do not resemble that of the absorption spectrum (top panel). Second, the profiles are not "nested", but rather show dramatic changes in their relative intensities as a function of the excitation wavelength. (The changes are more apparent in subsequent figures where the profiles are plotted on the same intensity scale.) The ratios of the intensities of the modes are not constant across the profiles. For example, the ratio of the 488-cm^{-1} mode to that of the 396-cm^{-1} mode at 15454 cm^{-1} is 0.3 but at 19436 cm^{-1} it is 6.9.

Absorption Spectroscopy. The 77 K polarized single-crystal absorption spectrum of CrOs is shown at the top of Figure 2 and in Figure 3 . The maximum of the intervalence absorption band is at 18 900 cm^{-1} and a shoulder is observed at 17 200 cm^{-1}. Both bands are strongly polarized and both have the same polarization direction. The absorption band was fit with two Gaussians to estimate the positions and magnitudes of the two components and is shown in Figure 3 (top). The first Gaussian has a maximum at 17 300 cm^{-1} and a width of 2150 cm^{-1}, while the second Gaussian has a maximum at 19 550 cm^{-1} and a width of 3850 cm^{-1}. The ratio of the heights of the two Gaussians is 1:2.1.

(23) Shin, K. S. K.; Zink, J. I. *J. Am. Chem. Soc.* **1990**, *112*, 7148.
(24) Reber, C.; Zink, J. I. *J. Phys. Chem.* **1992**, *96*, 571.
(25) Laidlaw, W. M.; Denning, R. G. *Polyhedron* **1994**, *13*, 2337.
(26) Chang, T. H.; Zink, J. I. *J. Am. Chem. Soc.* **1984**, *106*, 287.

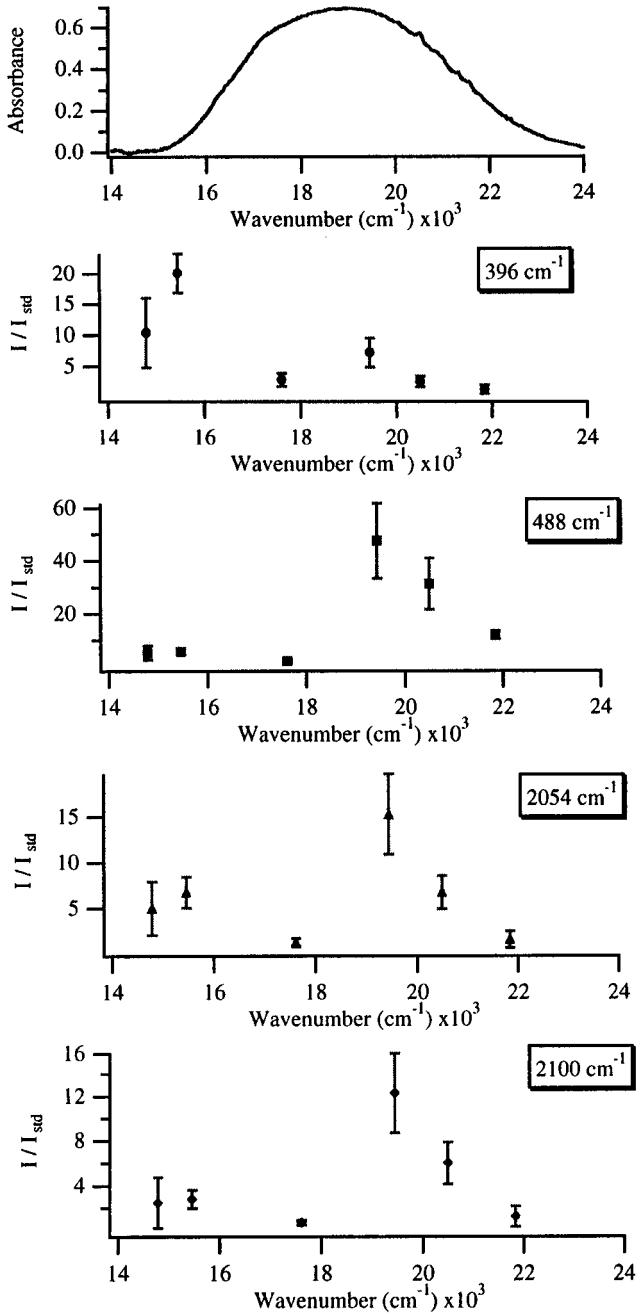

Figure 2. Experimental resonance Raman excitation profiles (bottom four panels). The band shapes of the profiles are very different from that of the electronic absorption spectrum (top panel).

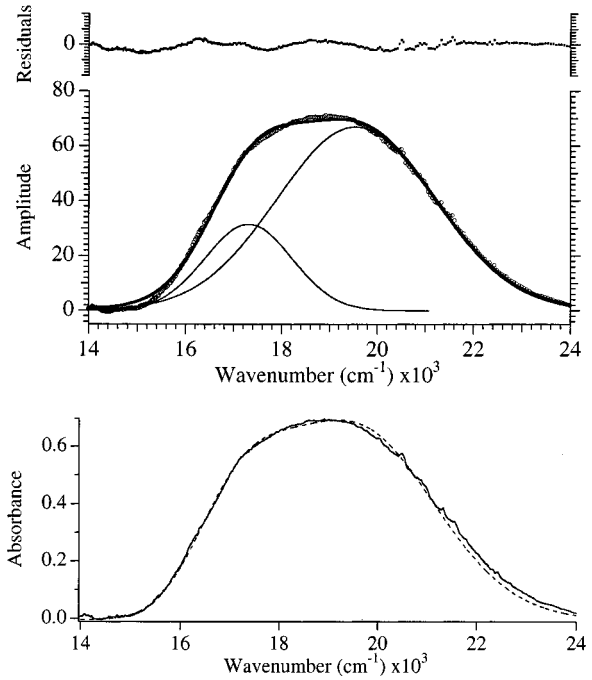

Figure 3. Top panels: polarized single-crystal absorption spectrum (solid lines) and the Gaussian fit to the two components. The difference is shown at the top. Bottom panel: absorption spectrum (dotted line), calculated by using the parameters from the fit to the experimental excitation profiles, superimposed on the experimental absorption spectrum.

Discussion

1. Single Crystal Absorption. Previous experimental and theoretical studies have shown that the presence of nearby electronic states leads to interference effects that can cause wavelength-dependent intensity ratio changes. To examine the possibility of overlapping transitions in CrOs, the low-temperature single-crystal polarized absorption spectrum was taken. Because the solution absorption spectrum has an extinction coefficient of 2200 $M^{-1}cm^{-1}$, thin crystals ($\sim$1.25 μm, grown between quartz plates) were necessary to keep the absorbance less than 2. The spectrum was recorded on an instrument previously described and is shown on the top of Figure 1 and in Figure 3. The absorption maximum is at 18 900 cm^{-1} (CH_3CN solution 18 060 cm^{-1}). Most importantly, at low temperature a shoulder is observed at 17 200 cm^{-1}. The absorption bands are strongly polarized and both components have the same polarization. The assignments of the two electronic states cannot be made definitively, even with the Raman data from this study. One possibility is that the two bands arise from transitions to two spin−orbit states of CrOs, similar to the literature assignment for the analogous OsOs complex.[23] Another possibility is that there is accidental near degeneracy between the filled b_2 and e orbitals on chromium leading to overlapping chromium to osmium electron transfer bands. Other accidental near degeneracies are possible, including overlap of chromium dπ → osmium dπ and osmium dπ → chromium dσ one-electron transitions. Although both the polarization data and the Raman data are least consistent with the spin−orbit assignment, electronic structure calculations will be needed to make a more definitive assignment.

2. Resonance Raman Spectroscopy. The resonance Raman bands of CrOs that show both the greatest enhancement and the greatest intensity difference as a function of excitation wavelength are the 396- and the 488-cm^{-1} vibrational modes. Resonance Raman spectra with two different excitation frequencies are shown in Figure 4. The intensity ratio of the vibrational mode at 396 cm^{-1} to the 488-cm^{-1} mode changes by more than a factor of 20. The next most prominent band, that at 2100 cm^{-1}, has a distortion of less than 10% of that of the former two. The theoretical treatment will focus on the two most intense and highly distorted bands and will include other bands for completeness.

Raman bands corresponding to Os−N vibrational modes are expected in the frequency region from 450 to 550 cm^{-1} and those to Cr−C in the 300−500-cm^{-1} region based on previous studies of substituted chromium pentacarbonyl and osmium pentaammine comparison compounds. The 488-cm^{-1} mode is assigned to either the bridging Os−N stretch or the axial NH_3−Os stretch. In $[Os(NH_3)_5X]X_2$ where X = Cl [27,28] three Os−N

(27) Bee, M. W.; Kettle, S. F. A.; Powell, D. B. *Spectrochim. Acta* **1974**, *30A*, 585.

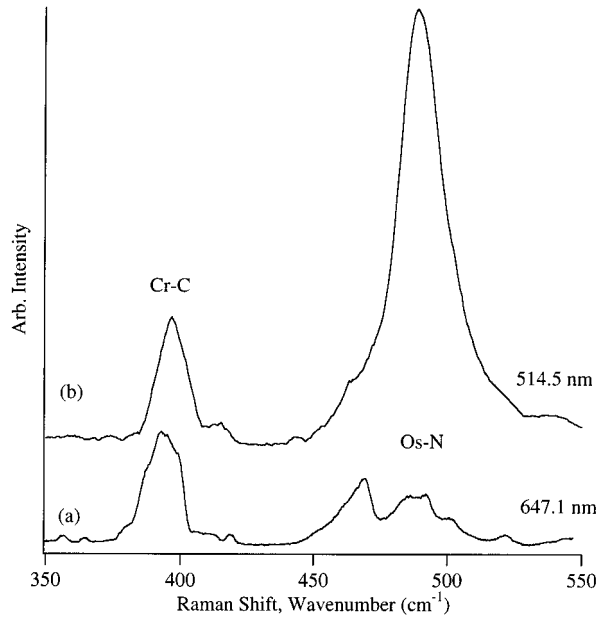

Figure 4. Resonance Raman spectra of CrOs in the metal−ligand region of 350−550 cm^{-1} excited at 647.1 (a) and 514.5 nm (b).

stretching frequencies were observed and assigned as follows: 504 cm^{-1} assigned as the a_1 Os−N equatorial stretch, 483 cm^{-1} assigned as the a_1 Os−N axial stretch, and 468 cm^{-1} assigned as the b_1 Os−N equatorial stretch. In the spectrum of CrOs excited with 647.1 nm (Figure 4), the mode at 469 cm^{-1} is assigned as the b_1 equatorial Os−N stretch and the mode at 500 cm^{-1} as the Os−N a_1 equatorial stretch. The 488-cm^{-1} mode is strongly enhanced whereas the 469- and 500-cm^{-1} modes are not. The orbital on Os that is involved in the electron transfer transition is a dπ orbital. Thus, the 488 cm^{-1} mode is probably primarily bridging Os−N in character, although the Os−NH_3 stretch cannot be ruled out.

The intense band at 396 cm^{-1} of CrOs can be assigned to either the bridging Cr−CN stretch or the equatorial Cr−CO stretch. In the related complex $Cr(CO)_5CS$, Raman bands assigned as Cr−C stretches of a_1 symmetry were observed at 424, 380, and 351 cm^{-1}.[29] The 424-cm^{-1} mode was assigned as the a_1 axial Cr−CO, the 380-cm^{-1} mode was assigned as the a_1 equatorial Cr−CO stretch, and the 351-cm^{-1} mode was assigned as the a_1 Cr−CS stretch.[29] In the Raman spectrum of $Cr(CO)_5$(CNBu-*t*), Cr−CO stretching frequencies were assigned at 436 and 393 cm^{-1} while a band at 368 cm^{-1} was assigned to the Cr−CN stretch.[30] In the IR spectrum of $[Cr(CO)_5CN]^-$ in CH_2Cl_2 solution, bands observed at 450 (E) and 427 (A_1) cm^{-1} were assigned as Cr−C stretches, but the Cr−CN stretch was not assigned.[31]

The two most intense bands in the high-frequency region are found at 2100 and 2054 cm^{-1}. The 2100-cm^{-1} band is assigned as the bridging cyanide stretch and the 2054-cm^{-1} band to the A_1 equatorial CO stretch. These assignments correspond to those made in the IR spectrum of CrOs[25] and by comparison with other Class II cyano bridged MMCT complexes.[11,12,14] There will be four Raman active carbonyl vibrations in C_{4v} symmetry: $2A_1 + B_1 + E$. In the spectrum of CrOs, the mode at 2054 cm^{-1} is assigned as the A_1 equatorial stretch, the mode at 1970 cm^{-1} as the A_1 axial stretch, the mode at 1917 cm^{-1} to the E stretch, and the mode at 1882 cm^{-1} to the B_1 stretch. In the related complex $[Cr(CO)_5CN]^-$ the IR spectrum in CH_2Cl_2 solution shows bands at 2112 (A_1 CN stretch), 2053 (A_1 CO stretch), 1930 (E CO stretch), and 1894 cm^{-1} (A_1 CO stretch).[31] In the Raman spectrum of solid $[Cr(CO)_5CN]^-$ the CN stretch was observed at 2102 cm^{-1} while bands assigned as CO stretches were observed at 2057, 1974, 1897, and 1879 cm^{-1} and a shoulder was observed at 1964 cm^{-1}.[32]

3. Resonance Raman Excitation Profiles. The resonance Raman excitation profiles for all of the vibrational modes show resonance de-enhancement. Using eq 1 to calculate the distortions will lead to inconsistent results because the resonance Raman intensities vary with the excitation wavelength. A method that considers interference between electronic states must be used to account for the resonance de-enhancement observed in the resonance Raman excitation profiles.

(a) Theoretical Methods. The resonance Raman excitation profiles were calculated with the time-dependent theory of spectroscopy considering interference between two electronic states.[23] Interference between states is interpreted by examining the constructive or destructive interference between the real and imaginary parts of the Raman scattering cross section. The resonance Raman intensity for two states is given by

$$I \propto (\alpha_1 + \alpha_2)^2 \tag{2}$$

The scattering cross section α for *n* electronic states is given by

$$\alpha_{fi} = \frac{i}{\hbar}\int_0^\infty \Big(\sum_{r=1}^{n} \mu_r^2 \langle\phi_f|\phi(t)\rangle_r \exp(-iE_{00}^{(r)}t - \Gamma_t^{(r)})\Big) \exp\{i(\omega_i + \omega_I)t\}\, dt \tag{3}$$

where μ is the transition dipole moment, E_{00} is the electronic origin, and Γ is a damping factor of the *r*th electronic state. The time-dependent overlap of the final function ϕ_f with the propagating wavepacket $\phi(t)$ is given by

$$\langle\phi_f|\phi(t)\rangle = \prod_k \left\{ \exp\left[-\frac{\Delta_k^{\,2}}{2}(1 - \exp(-i\omega_k t)) - \frac{i\omega_k t}{2} \right] \times (1 - \exp(-i\omega_k t))^{n_k} \frac{(-1)^{n_k}\,\Delta_k^{\,n_k}}{(2^{n_k} n_k!)^{1/2}} \right\} \tag{4}$$

where Δ_k is the distortion, ω_k is the vibrational frequency, and n_k is the order of the *k*th normal mode. The effects of μ, Δ, E_{00}, and Γ on interference effects in resonance Raman excitation profiles have been derived.[23] Note that the Raman intensities are proportional to the square of the sum of the Raman cross sections (eq 2), not just to the sum of the squares from both states. Also note that calculations involving multiple normal modes must simultaneously include all of the modes (eq 4).

(b) Two Mode Fit. Quantitative calculations of the Raman profiles and the wavelength-dependent intensity ratios are subject to limiting constraints. Not only must the intensities be accurately calculated, but also the experimental absorption spectrum must be accurately calculated, and the parameters must be physically meaningful. The simultaneous fit of both the electronic spectra and the Raman excitation profiles places severe limits on the values of μ, Δ, and E_{00}.

(28) Bee, M. W.; Kettle, S. F. A.; Powell, D. B. *Spectrochim. Acta* **1974**, *30A*, 139.
(29) English, A. M.; Plowman, K. R.; Butler, I. S. *Inorg. Chem.* **1981**, *20*, 2553.
(30) Li, H.; Butler, I. S.; Uhm, H. L. *J. Raman Spectrosc.* **1992**, *23*, 457.
(31) Lindler, E.; Behrens, H. *Spectrochim. Acta* **1967**, *23A*, 3025.
(32) Fritz, M.; Rieger, D.; Bar, E.; Beck, G.; Fuchs, J.; Holzmann, G.; Fehlhammer, W. P. *Inorg. Chim. Acta* **1992**, *200*, 513.

Table 1. Parameters Used in Two-Mode and Three Mode Fits

parameter	electronic state 1	electronic state 2
	Two-Mode Fit	
Δ_{396}	2.20	0.78
Δ_{488}	1.00	1.80
E_{00}	14700	18400
Γ, cm^{-1}	420	780
μ	1.00	1.55
	Three-Mode Fit	
Δ_{396}	2.20	1.00
Δ_{488}	1.30	2.50
Δ_{2100}	0.17	0.27
E_{00}, cm^{-1}	14500	17000
Γ, cm^{-1}	400	750
μ	1.00	1.7

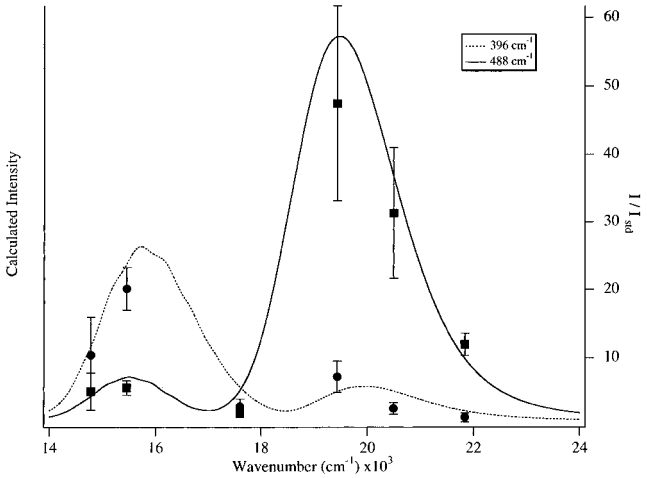

Figure 5. Calculated resonance Raman excitation profiles for the 396- (dotted line) and 488-cm^{-1} (solid line) normal modes. The experimental data points for the modes are indicated by circles and squares, respectively. The distortions and other parameters are given in the table.

The resonance Raman excitation profiles for the 396-cm^{-1} Cr−CN bridging stretch and the 488-cm^{-1} Os−NC bridging stretch can be fit with a two electronic state model. The two vibrational modes were chosen because they have the largest distortions and also show the most drastic changes in the intensity ratios. The maximum intensity ratio change is more than a factor of 20. The parameters used in the fit are given in Table 1 and the calculated fits to the experimental excitation profiles are shown in Figure 5. This two electronic state, two-vibrational mode model gives an excellent fit to both the experimental excitation profiles and the absorption spectrum.

(c) Three Mode Fit. In order to examine the effects of including other normal modes in the model, the 2100-cm^{-1} bridging CN mode was incorporated. This mode was chosen for three reasons: it shows the third strongest resonance enhancement (after the 396- and 488-cm^{-1} modes), it is assigned to the CN bridging ligand stretch and is thus closely linked with the former two distortions, and its profile shows a small dip and thus is affected by the two electronic states. The best three-mode fit of the experimental profiles is shown in Figure 6. The parameters used in the fit are given in Table 1. It is interesting to note that the inclusion of another mode in the fit does not significantly change the parameters for the 396- and 488-cm^{-1} modes that were used in the two-mode fit. This result is common in fits to excitation profiles involving one electronic state; inclusion of more modes with smaller distortions causes only small changes in the values of Δ and Γ. The electronic absorption spectrum that is calculated by using exactly the

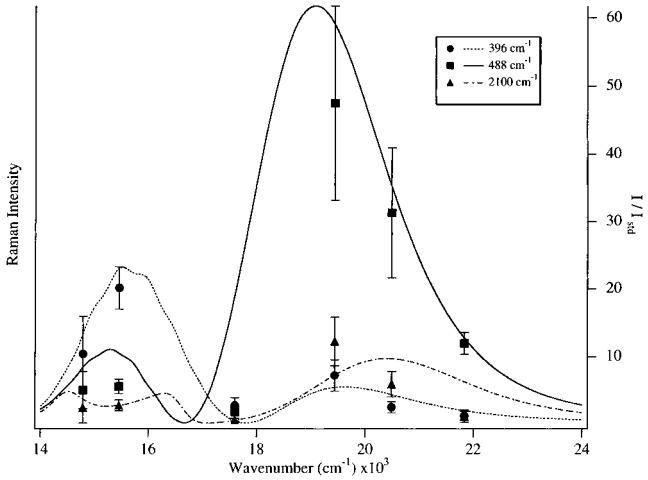

Figure 6. Calculated resonance Raman excitation profiles and experimental data points for the 396-cm^{-1} mode (dotted line, circles), the 488-cm^{-1} mode (solid line, squares), and the 2100-cm^{-1} mode (dash-dot line, triangles). The parameters are given in the table and the calculated absorption spectrum is shown in Figure 3.

parameters that were used in the fit to the profiles is shown in the bottom panel of Figure 3. An excellent fit is also obtained. The simultaneous fitting of the resonance Raman profiles and the electronic absorption spectrum is evidence for not only the meaningfulness of the model but also the power of the time-dependent theory of resonance Raman spectral intensities with two interfering electronic states. The origin of the interference, the physical meaning of the parameters, and the uniqueness of the fit are discussed below.

(d) Origin of the Interference. The factors contributing to the dramatic changes in the ratios of the Raman intensities can be interpreted by examining the real and imaginary parts of the Raman cross section. The components for the 488-cm^{-1} normal mode are shown in Figure 7. The imaginary part peaks at about the position of the maximum of the absorption band whereas the real part changes sign at that wavenumber. The square of the sum of these two components gives the excitation profile. When two electronic states are in close proximity, the real and the imaginary parts of the cross sections of both states are added and then squared to obtain the profile. In Figure 7, the negative component of the real part from the lowest energy state reaches its most negative value at about 17 000 cm^{-1} whereas the positive component of the real part from the higher energy state reaches its maximum at just about that energy (17 600 cm^{-1}). The sum of these two oppositely-signed components leads to a large cancellation in the 17000-cm^{-1} region and a correspondingly large decrease in the Raman intensity. The imaginary parts do not undergo such drastic cancellations. The net result (the square of the sums) is a large decrease in the Raman intensity at around 17 000 cm^{-1} caused by the destructive interference compared to that in the other regions of the profile.

The explanation for the opposite pattern of Raman intensity at 396 cm^{-1} is similar, but in this case the magnitudes of the real and imaginary parts from the two states are different. Thus the cancellation in the 17 000-cm^{-1} region is not as pronounced whereas the cancellation from the negative "wings" of the real part with the positive peak in the 19 000-cm^{-1} region is more pronounced. The next result is that "dip" in the profile is shifted to slightly higher wavenumber and the intensity in the high-wavenumber region of the spectrum is dramatically decreased.

The interference effects discussed above are closely related to resonance de-enhancement and the explanation is similar. However, the familiar examples of resonance de-enhancement

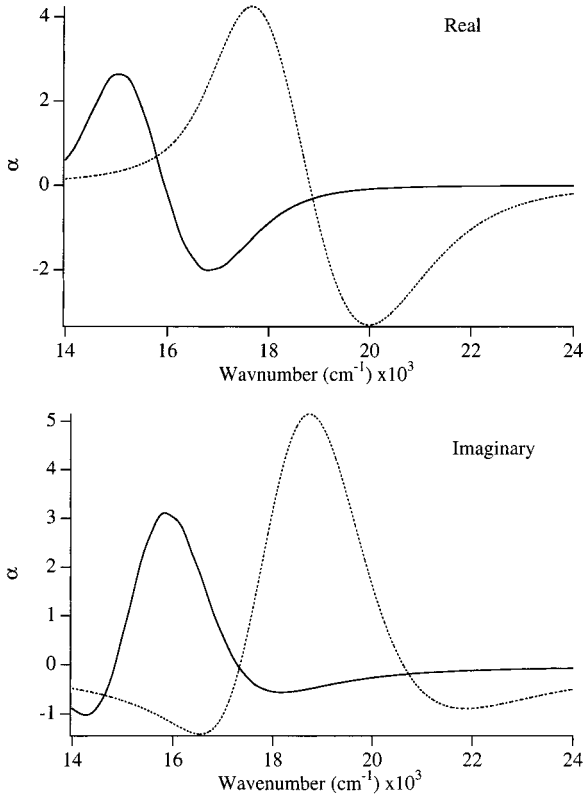

Figure 7. The contributions to the real (top panel) and imaginary (bottom panel) parts of the polarizability for the 488-cm^{-1} normal modes from the two electronic states.

require the special conditions that the two interfering states have very different magnitudes of their transition dipole moments, and that the states are well-enough separated in energy such that the *wing* from the intense band is about the same in magnitude but opposite in sign from the *maximum* of the corresponding component from the less intense transition. In these particular cases, the de-enhancement appears as a dip at a wavenumber near the maximum of the weak absorption band.

In our calculations we have shown that interference occurs between electronic states within the MMCT absorption band. The possibility of interference between the MMCT absorption band and the higher energy MLCT absorption bands was also examined. However, these states have such a large energy separation that the interference effects are negligible.

(e) Physical Meaning of the Distortions. The conversion of the distortions of the modes into angstrom units requires a knowledge of the **F** and **G** matrices. As a rough estimate, when the mass of the ligand is taken as 27 and the normal mode is assumed to involve only the motion of the ligand, the distortions for the 396-cm^{-1} mode are 0.12 Å in the first state and 0.06 Å in the second state, that for the 488-cm^{-1} mode is 0.06 Å in the first state and 0.13 Å in the second state, and that for the 2100-cm^{-1} mode is 0.004 Å in the first state and 0.006 Å in the second state. Inclusion of more vibrational modes scales the values of the distortions smaller but does not strongly affect the calculated ratios. Because of the large number of parameters required for modeling two electronic states, the fit is not unique and a variety of different parameters can be used to fit the observed intensity ratios. The constraints discussed above limit the range of the parameters; generally a variation of the parameters by more than a factor of 1.5 results in a significantly poorer fit.

Conclusions

The unusual wavelength-dependent resonance Raman intensity ratios observed in $[(CO)_5Cr^0-CN-Os^{III}(NH_3)_5](CF_3SO_3)_2$ (CrOs) cannot be explained by scattering from only one electronic state, and the use of eq 1 to estimate bond distortions and the mode-specific inner sphere vibrational reorganization energies is not valid. However, the profiles and intensity ratios can be calculated by using the time-dependent theory and by including the interference between two electronic states that are observed in the low-temperature polarized single-crystal absorption spectrum of CrOs. The broad, unresolved electron transfer absorption bands frequently observed in metal-containing compounds may contain more than one transition. The resonance Raman intensities can reveal their presence, and the quantitative calculations can provide detailed information about both the states and the distortions.

Acknowledgment. This work was made possible by a grant from the National Science Foundation (CHE-9509275). We thank Prof. David Bocian for enabling us to obtain the spectrum at 568.2 nm when our laser no longer produced that line.

JA962228L